PCCP

Physical Chemistry Chemical Physics

ROYAL SOCIETY
OF **CHEMISTRY**
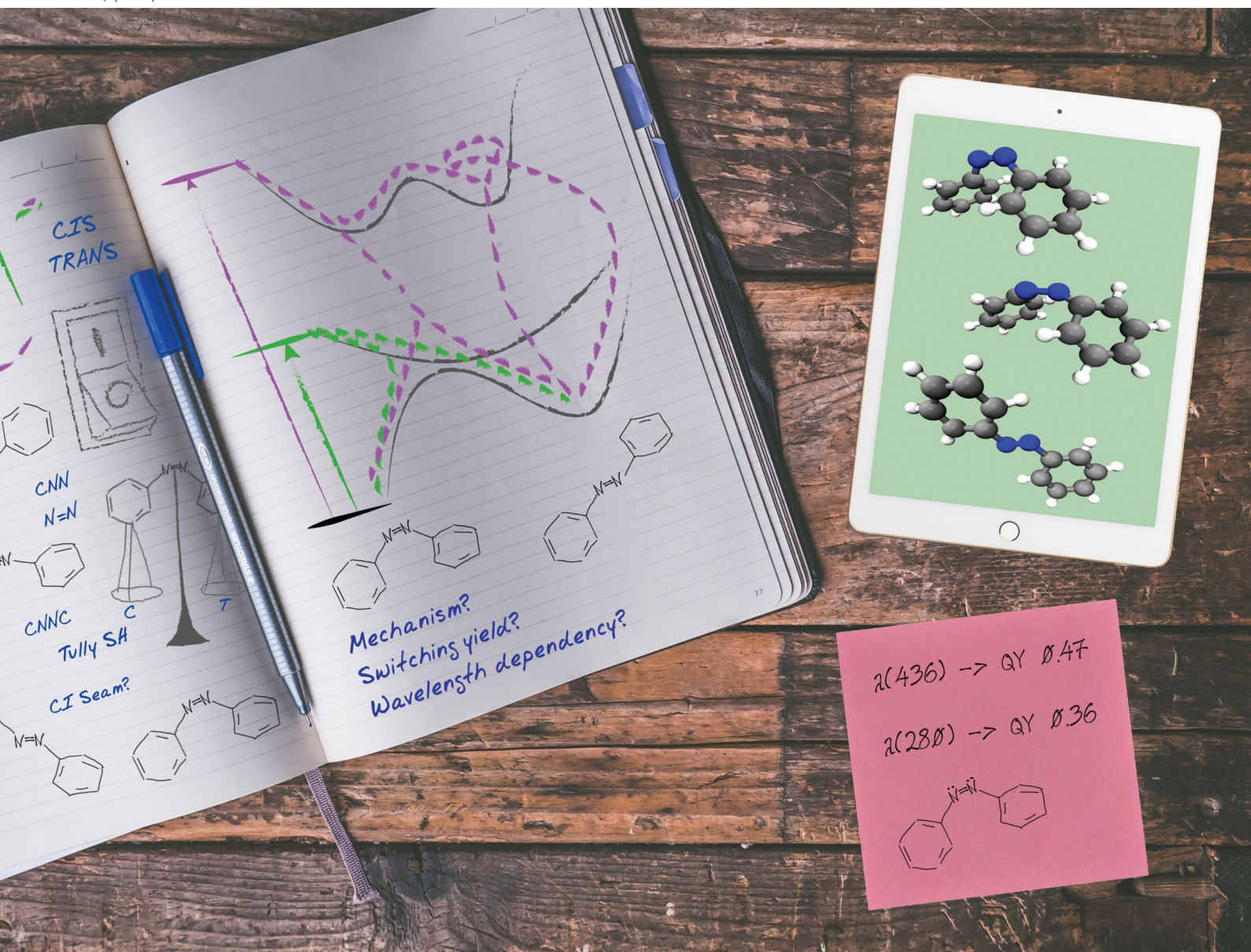
PAPER
Morgane Vacher *et al.*
cis → trans photoisomerisation of azobenzene: a fresh
theoretical look

Check for updates

cis → trans photoisomerisation of azobenzene: a fresh theoretical look†

Isabella C. D. Merritt, [ID] Denis Jacquemin [ID] and Morgane Vacher [ID] *

The *cis* → *trans* photo-isomerisation mechanism of azobenzene, after excitation to the nπ* and ππ* states, is revisited using high-level *ab initio* surface hopping mixed quantum-classical dynamics in combination with multi-reference CASSCF electronic structure calculations. A reduction of photoisomerisation quantum yield of 0.10 on exciting to the higher energy ππ* state compared to the lower energy nπ* state is obtained, in close agreement with the most recent experimental values [Ladányi *et al.*, *Photochem. Photobiol. Sci.*, 2017, **16**, 1757–1761] which re-examined previous literature values which showed larger changes in quantum yield. By direct comparison of both excitations, we have found that the explanation for the decrease in quantum yield is not the same as for the reduction observed in the *trans* → *cis* photoisomerisation. In contrast to the *trans* → *cis* scenario, $S_1 \to S_0$ decay does not occur at 'earlier' C–N=N–C angles along the central torsional coordinate after ππ* excitation, as in the *cis* → *trans* case the rotation about this coordinate occurs too rapidly. The wavelength dependency of the quantum yield is instead found to be due to a potential well on the S_2 surface, from which either *cis* or *trans*-azobenzene can be formed. While this well is accessible after both excitations, it is more easily accessed after ππ* excitation – an additional 15–17% of photochromes, which under nπ* excitation would have exclusively formed the *trans* isomer, are trapped in this well after ππ* excitation. The probability of forming the *cis* isomer when leaving this well is also higher after ππ* excitation, increasing from 9% to 35%. The combination of these two factors results in the reduction of 0.10 of the quantum yield of photoisomerisation on ππ* excitation of *cis*-azobenzene, compared to nπ* excitation.

1 Introduction

Photoswitches are molecules that can be interconverted between two or more stable isomeric forms, using light for at least one direction of switching. They are of high interest in a wide range of fields – with applications ranging from biology[1] to material science.[2] Being one of the simplest photochromes, azobenzene (AZB) is considered to be an 'archetypical' molecular switch[3] – its reversible isomerisation as shown in Scheme 1 between its *trans* (*E*) and *cis* (*Z*) forms around the central N=N double bond being a prototype for *E–Z* type photochromism. A number of favourable properties also explain AZBs' popularity: excellent fatigue

resistance,[4] a large geometry change upon isomerisation,[5] photoactivity even under constrained conditions,[6–8] and easily accessible chemical substitutions to tune its properties.[1,9,10]

Morgane Vacher is currently working as a CNRS researcher at the University of Nantes (France), within the CEISAM laboratory. She received in 2016 her PhD degree in theoretical and computational chemistry from Imperial College London (United Kingdom), supervised by Profs Mike Robb and Mike Bearpark. She worked then as a postdoctoral researcher at Uppsala University (Sweden), within the group of Prof. Roland Lindh. Since late 2019, she was appointed as a CNRS researcher. Her research interests include theoretical photochemistry and non-adiabatic dynamics of molecular excited states using direct ab initio methods, and the application of attosecond science to chemistry.

Morgane Vacher

Laboratoire CEISAM – UMR 6230 – CNRS – Université de Nantes, Nantes, France.
E-mail: morgane.vacher@univ-nantes.fr; Tel: +33-2-76-64-51-47

† Electronic supplementary information (ESI) available: Full active space orbital descriptions; (ii) geometrical coordinates of critical points; (iii) basis set convergence test; (iv) CASSCF *vs.* CASPT2 energies and state ordering; (v) rigid potential energy scans along central torsional coordinate; (vi) convergence of simulations with number of trajectories; (vii) energy conservation with timestep chosen for trajectories; (viii) additional dynamics plots – electronic populations, internal coordinates, justification of reactive/non-reactive trajectory assignment, and hopping geometry characterisation. (ix) Model trajectories for different pathways. See DOI: 10.1039/d1cp01873f

This journal is © the Owner Societies 2021

Phys. Chem. Chem. Phys., 2021, **23**, 19155–19165 | 19155
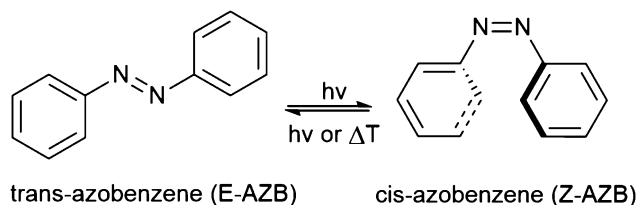
Scheme 1 Azobenzene *trans* ⇌ *cis* isomerisation.

However, there are some unfortunate drawbacks to AZBs. The absorption spectra of the *cis* and *trans* isomers are significantly overlapping, leading to the formation of stationary states containing a significant mix of isomers. The *cis* → *trans* back-reaction also occurs thermally, with a half-life at room temperature of around 2 days;[9] meaning AZB cannot be used as a permanent switch. Finally, the wavelength of light used for *trans* → *cis* switching lies in the UV region and can cause cell damage in biological applications.[1] Substitutions of AZBs are often used to circumvent one or more of these drawbacks.[21–23] However, choosing the appropriate substitutions from the immense pool of available ones is challenging.

To optimise AZB derivatives for applications, it is essential to first have an accurate understanding of the photophysical processes involved in the photo-switching reaction. Even unsubstituted AZB offers a rich and complex photophysics, not easily understood by experiment nor theory. The mechanism followed after photoexcitation was a main topic of research for most of the history of AZBs. Historically, the isomerisation of AZB was proposed to proceed *via* rotation or inversion mechanisms. Pure rotation or inversion are extreme pictures oversimplifying the reality. The photoisomerisation mechanism of AZB is now accepted to proceed *via* an "inversion-assisted torsion" mechanism along a torsional coordinate around the central C–N=N–C, assisted by C–N=N bending modes.[24,25] A refined version of the mechanism is sometimes called "pedal motion" in the literature.[26] Indeed, during the isomerisation, the phenyl rings remain roughly stationary, while the central C–N=N–C moiety rotates and moves between them in a pedal-type motion. The phenyl rings do also move into plane, however they move on a much slower timescale than the central moiety. As a result, they are still out of plane once the isomerisation has occurred, *i.e.*, when the central CNNC dihedral angle has reached 180, and they continue to twist after the main isomerisation event has finished. It is noted that, in some cases, a "hula-twist" mechanism is invoked to explain *cis–trans* photoisomerisation reactions.[27] In that model, two adjacent bonds (a pair of double and single bonds) twist concertedly.

One of the most interesting properties of AZB (sometimes referred to as Kasha's rule breaking in the literature)[9,24,28–30] is the dependence of the measured quantum yield (QY) on the wavelength of the incident light used to trigger the photo-isomerisation. There have been numerous theoretical contributions focusing on the *trans* → *cis* isomerisation of AZB,[18,24,25,29–34] since applications of these photochromes make use of this photoisomerisation direction, while the reverse *cis* → *trans*

isomerisation often relies on a thermal pathway. The QY of the *trans* → *cis* isomerisation $\phi_{t \to c}$ upon excitation at $\sim$450 nm to the nπ^* S$_1$ state is *ca.* 0.25, while $\phi_{t \to c}$ upon irradiation at $\sim$320 nm to the $\pi\pi^*$ S$_2$ state is only *ca.* 0.12.[14] This clear wavelength dependency of the QY has been studied a great deal, and reasonable explanations have been proposed.[18,29,30] While there still exists debate over exact details of the wavelength dependency of the *trans* → *cis* photoisomerisation,[24,29,33] the generally accepted explanation is that upon excitation to the $\pi\pi^*$ S$_2$ state, the additional vibrational energy present (compared to nπ^* S$_1$ excitation) allows the S$_1$/S$_0$ decay to occur at higher energies. Indeed, additional vibrational energy is present in the C–N=N modes (in particular in the asymmetric bending mode). This allows for decay to the ground state through a higher energy section of the S$_1$/S$_0$ conical intersection seam than is accessible after nπ^* S$_1$ excitation. This part of the seam corresponds to values of the central dihedral angle closer to 180, earlier along the C–N=N–C torsional coordinate.[18,29,30] As a result, the *trans* isomer is preferentially formed, as the C–N=N–C is closer to 180 in the ground state – reducing the quantum yield of *trans* → *cis* isomerisation.

The *cis* → *trans* photo-isomerisation has been much less investigated, with fewer theoretical studies dedicated to this process.[18,20,25,35–38] Of these, even fewer[18,20] investigate isomerisation after excitation at different wavelengths to both the nπ^* and $\pi\pi^*$ states (see below). The QYs for the *cis* → *trans* isomerisation are in general higher than those of *trans* → *cis*,[39] but the dependency of QY on wavelength is less clear, varying notably from study to study. A summary of literature QYs for the *cis* → *trans* isomerisation from S$_1$ and S$_2$ is given in Table 1. To the best of our knowledge, the most recent measurements of the quantum yields of unsubstituted AZB were carried out in 2017,[17] highlighting that the QYs of *cis*-AZB are still open to debate.

From Table 1, it is clear that the level to which $\phi_{c \to t}$ is reduced on exciting at a shorter wavelength is not fully agreed upon, with the most recent study giving $\phi_{c \to t}$ of 0.47 (S$_1$) and 0.36 (S$_2$).[17] – a reduction of 0.11 only, much less than the reduction of 0.29 measured previously in the same solvent.[15] In ref. 17, the differences in QYs from previous literature values were attributed to the reference absorbance spectrum used for the *cis* isomer – the *cis*-AZB spectra used prior to that study seemed to contain non-trivial amounts of the *trans* isomer. There are also other possible explanations for the variations in QYs found in literature. For instance, the irradiation wavelength that is used to excite to S$_2$ may have an effect – studies on AZB often use radiation in the 310–340 nm range for both isomers.[12–14,16] This matches the maximum of the $\pi\pi^*$ band of *trans* AZB, however the *cis* AZB $\pi\pi^*$ maximum is in fact found at 280 nm.[40]

While the *cis* → *trans* isomerisation mechanism is generally agreed to proceed *via* a rotation-based mechanism, like that of the *trans* → *cis*, there are still some uncertainties in the specifics of this mechanism. Studies into the isomerisation of AZB typically assume that the fundamental explanation of the wavelength dependence of QYs for *cis* → *trans* isomerisation is the same as for *trans* → *cis*.[18,24,35] However, while some studies have found that the S$_1$/S$_0$ intersection accessed during the

19156 | *Phys. Chem. Chem. Phys.*, 2021, **23**, 19155–19165

This journal is © the Owner Societies 2021

Table 1 Literature values for the quantum yield of *cis* → *trans* isomerisation ($\phi_{c \to t}$) after excitation to the $S_1(n\pi^*)$ and $S_2(\pi\pi^*)$ states at the given irradiation wavelengths (λ_{irr}). TSH stands for trajectory-based surface hopping

Experimental studies	Solvent	$\phi_{c \to t}$ nπ^*	$\phi_{c \to t}$ $\pi\pi^*$	nπ^* λ_{irr} (nm)	$\pi\pi^*$ λ_{irr} (nm)
Zimmerman *et al.*[11] (1958)	Isooctane	0.46–0.55	0.44	436	313
Malkin and Fischer[12] (1962)	Isohexane	0.4	0.4	436	313
Ronayette *et al.*[13] (1974)	Cyclohexane	0.55	0.42	436	313
	Isopropanol	0.42	0.50	436	313
Bortolus *et al.*[14] (1979)	*n*-Hexane	0.56	0.24	439	317
Gauglitz and Hubig[15] (1985)	Methanol	0.63	0.34	436	280
Quick *et al.*[16] (2014)	Hexane	0.55	0.31	444	310
Ladányi *et al.*[17] (2017)	Methanol	0.47	0.36	436	280

Theoretical studies	Dynamics method/electronic structure	$\phi_{c \to t}$ nπ^*	$\phi_{c \to t}$ $\pi\pi^*$
Persico *et al.*[18] (2004)	TSH/semi-empirical PES	0.61	0.48
Zhu *et al.*[19,20] (2015)	TSH/SA-CASSCF(6,6)	0.39	0.30–0.45

cis → *trans* isomerisation is the same as in the *trans* → *cis*,[25,33] others reported different S_1/S_0 intersections along the rotational isomerisation path depending on the initial AZB isomer.[20,24] There is even some experimental evidence suggesting that after $\pi\pi^*$ excitation, the *cis* → *trans* isomerisation could occur rapidly *via* a S_2/S_1 conical intersection, forming *trans*-AZB in its S_1 state.[16] The potential differences in isomerisation mechanism for the two photoswitching directions, and the variation in measured QYs for the *cis* → *trans* isomerisation, call into question the assumption that the same mechanism is at play in the two isomers to explain the reduction in QY when exciting to the $\pi\pi^*$ state.

Let us now briefly review previous theoretical works focused on the *cis* → *trans* back-photoisomerisation mechanism, which include excitation to both nπ^* (S_1) and $\pi\pi^*$ (S_2) states. The first work we are aware of, by Persico and coworkers,[18] used a mixed quantum-classical surface hopping approach with semi-empirical potential energy surfaces to study both the *trans* → *cis* and *cis* → *trans* isomerisations of AZB after both excitations. They found that for the *trans* → *cis* isomerisation after $\pi\pi^*$ excitation, the S_1/S_0 crossing occurred significantly earlier along the C–N═N–C torsion coordinate compared to after nπ^* excitation. However, they did not provide definitive conclusions whether this was also the case for the *cis* → *trans* isomerisation.

A decade later Zhu and coworkers,[19,20] as part of the development of a new surface-hopping algorithm where the hopping probability requires only adiabatic electronic energies and gradients, carried out *ab initio* SA-CASSCF(6,6) trajectory surface hopping calculations on the *cis* → *trans* isomerisation. They performed these calculations for both nπ^* and $\pi\pi^*$ excitations in two separate works, but apparently did not directly compare the two obtained QYs: $\phi_{c \to t}$ = 0.39 for nπ^* and $\phi_{c \to t}$ = 0.3–0.45 for $\pi\pi^*$ excitation. While the method they developed clearly reproduced the experimental QY trends when they studied the *trans* → *cis* isomerisation – with $\phi_{t \to c}$ = 0.33 for nπ^* and $\phi_{t \to c}$ = 0.11–0.13 for $\pi\pi^*$ excitations, it could not reproduce the expected difference in QYs between the two excitations for *cis* → *trans*.[19,34]

Striving to reach a more accurate and complete description of the *cis* → *trans* photoisomerisation of AZB after excitations to both excited states, we use here advanced *ab initio* methods. The present study aims to: (i) solve the apparent disagreement between the measured QYs, and test whether theoretical simulations fit better to the most recent measurements;[17] (ii) test the assumption that the same mechanism explains reduction in QY for both isomerisation directions; (iii) offer insight into the measured wavelength dependence of the *cis* → *trans* QY.

2 Methods

State-average complete active space self consistent field (SA-CASSCF)[41] calculations were used to explore the electronic structure of AZB. An active space of 14 electrons in 12 orbitals (14,12) was selected – consisting of the 2 N lone pairs, the 1 π & 1 π^* orbitals of the central N═N bond, and 4 each of the π & π^* orbitals mostly localised on the phenyl rings (full orbital descriptions can be found in Table S1 in the ESI†). A state-average over 4 states was chosen since the S_2 and S_3 states are close in energy (0.46 eV difference at the CASSCF level) at the *cis*-AZB ground state geometry. The relativistic core-correlated atomic natural orbital (ANO-RCC) basis set[42] with polarized double-zeta contraction (ANO-RCC-VDZP) was used. The sensitivity of our results with respect to the basis set was tested with ANO-RCC-VTZP, and the differences in transition energies obtained upon increasing the size of the basis set are less than 0.02 eV (see Table S6 in the ESI†). Resolution-of-identity based on the Cholesky decomposition was used throughout to speed up calculations.[43]

While SA-CASSCF is a method known to reproduce the potential energy surfaces of excited states with a reasonable description of the static (long-range) electron correlation, it is known that CASSCF may fall short due to the exclusion of the dynamic (short-range) electron correlation. Dynamic correlation can not only affect the excitation energy but also the shape of the potential energy surfaces. For instance, a theoretical study showed that vibrational frequencies in the S_1 state of the *trans*-AZB differ when including dynamic correlation.[44] The reliability of non-adiabatic dynamics simulations is highly dependent on the potentials used, *i.e.*, on the electronic structure method. It is thus important to establish that the SA-CASSCF method chosen is able to (at least) qualitatively describe the potential surfaces involved. The sensitivity of the electronic structure with respect to adding dynamic correlation was tested through second-order perturbation

theory with the CASPT2 method.[45] Importantly, the state ordering of the first 4 states for the *cis*-AZB isomer was the same at both CASSCF and CASPT2 levels (see Tables S7 and S8 in the ESI† for details). We also compared the SA4-CASSCF (used in this work) to MS-CASPT2 energies along the central torsional coordinate, as shown in Fig. S1 in the ESI:† the chosen CASSCF method can qualitatively reproduce the shapes of the potential energy surfaces, in particular around the Franck–Condon region and around $-90°$ where the lowest three states are close in energy and coupling vectors (and thus surface hopping probabilities) are expected to be high. As a result, we expect the surfaces used in this work to give qualitatively correct dynamics.

Initial conditions for dynamics were generated with Newton-X[46] for 100 trajectories, with geometries and velocities sampled (in an uncorrelated fashion) from the Wigner distribution using harmonic frequencies calculated at the SA4-CASSCF(14,12)/ANO-RCC-VDZP level of theory at the optimised ground-state equilibrium *cis*-AZB geometry. Convergence of the results for this number of trajectories was tested and can be found in the ESI† (Fig. S5).

Ab initio surface-hopping mixed quantum-classical dynamics were carried out using OpenMolcas,[47] employing the Tully fewest-switches surface hopping (FSSH) algorithm[48] along with the Hammes-Schiffer/Tully scheme,[49] and the decoherence correction as given by Persico and Granucci.[50] A timestep of 20 a.u. (0.48 fs) was chosen for the integration of Newton's equations using the Velocity-Verlet algorithm, with 96 substeps per timestep – energy conservation with this timestep was checked and can be found in the ESI† (Fig. S6). At each timestep, energies and gradients were computed at the SA4-CASSCF(14,12)/ANO-RCC-VDZP level of theory. Trajectories were initiated in the S_1 and S_2 states at the sampled geometries and velocities, and run for 550 fs.

3 Results and discussion

3.1 Electronic populations

Fig. 1a and b show the population of electronic states throughout the dynamics simulations, after excitation to the $n\pi^*$ (S_1) and the $\pi\pi^*$ (S_2) states respectively.

After S_1 excitation, the electronic population is rapidly transferred to S_0 with a S_1 state lifetime of 74 ± 1 fs. This value for the lifetime is in line with those determined in previous theoretical studies on the S_1 excitation of *cis*-AZB (67 fs,[37] 54 fs[19]), and has the same order of magnitude as the available experimental estimate (100 fs[16]).

The changes in electronic population after S_2 excitation are more complicated, and can be separated into different cases depending on what occurs in the first 20 fs following absorption. Around 45% of the trajectories undergo ultrafast decay to the S_1 state within 20 fs, after which transfer from the now populated S_1 state to the S_0 state begins. Another 45% of trajectories remain in the S_2 state after 20 fs, not undergoing this rapid electronic decay. The remaining 10% of trajectories transfer rapidly to the S_3 state, a $\pi\pi^*$ state lying only slightly higher in energy than S_2 at the Franck–Condon point. The electronic populations of the trajectories in the S_1 and S_2 states after 20 fs are shown in Fig. 2.[51]

For the trajectories that undergo rapid $S_2 \rightarrow S_1$ decay, the decay of the resulting S_1 state matches almost exactly that after direct excitation to the S_1 state, with a lifetime of 68 ± 1 fs. This is clearly shown by comparing the S_1 state (orange) on Fig. 1(a) and 2(a) (these two state populations are also plotted together for direct comparison in Fig. S7 in the ESI†). The two decays match very closely, and so this set of $\pi\pi^*$ trajectories follows an equivalent relaxation pathway as after initial S_1 excitation.

In contrast, Fig. 2b shows the changes in electronic population for the 45% of trajectories that are still in the S_2 state after 20 fs – those that do not undergo rapid $S_2 \rightarrow S_1$ transfer. The lifetime of the S_2 state for these trajectories is significantly longer, around 133 ± 2 fs, and the population of the S_0 state roughly mirrors that of S_2. Since $S_2 \rightarrow S_0$ hopping is not observed in the trajectories, this is interpreted as an almost immediate $S_1 \rightarrow S_0$ transfer following the slower $S_2 \rightarrow S_1$ transfer.

Finally, the remaining 10% of trajectories are those that rapidly transfer to the S_3 state within the first 20 fs. The S_3 state is close in energy to the S_2 state at the *cis* conformation, only 0.50 eV (0.13 eV) above at the CASSCF (CASPT2) level. The possibility of transfer to this state is therefore conceivable, and an equivalent S_3 $\pi\pi^*$ state has been theorised to play a role in
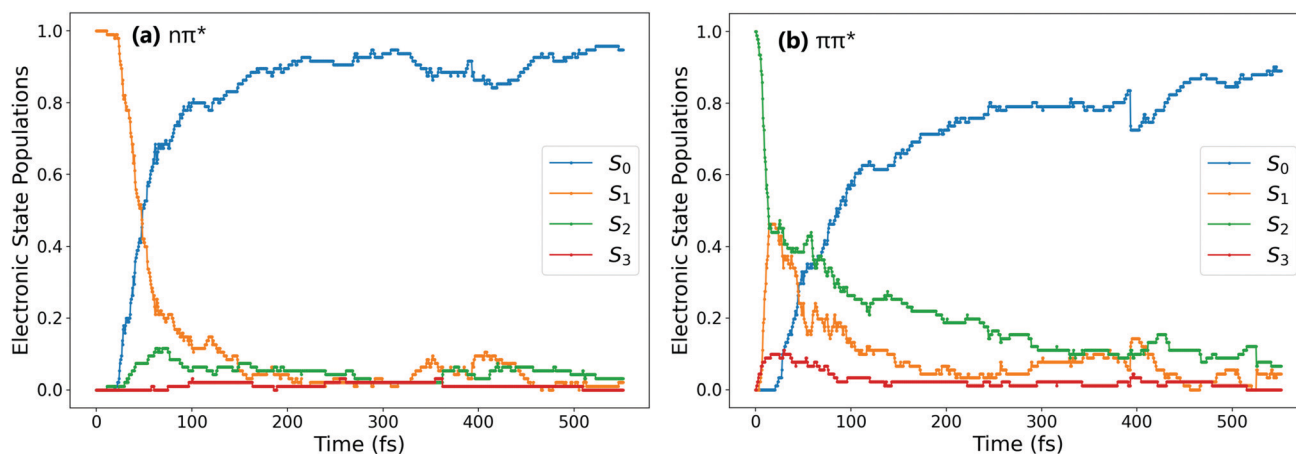

Fig. 1 Evolution of electronic state populations after excitation to (a) $n\pi^*$ and (b) $\pi\pi^*$ states.
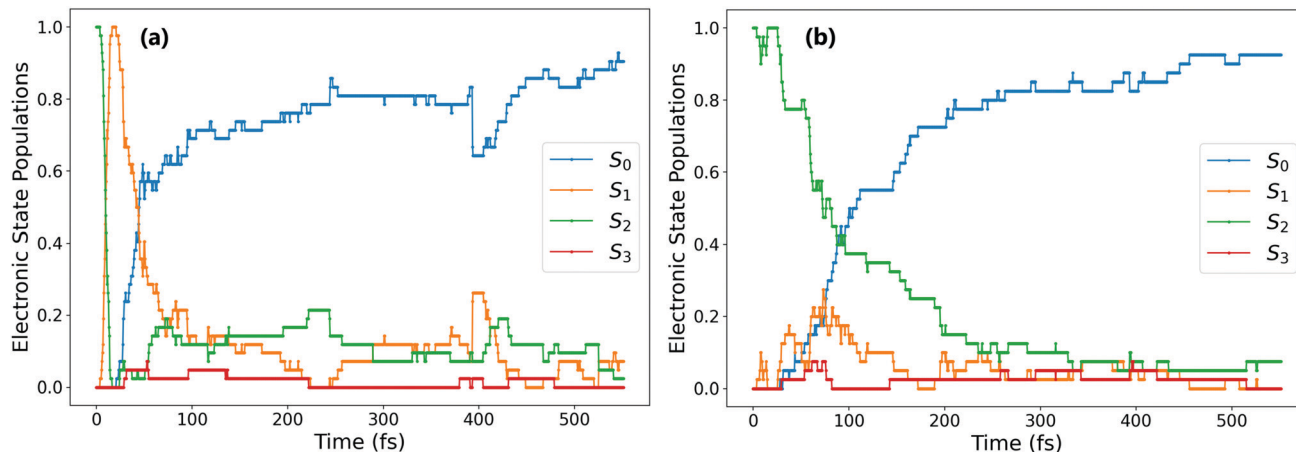
Fig. 2 Comparing evolution of electronic state population for two electronic pathways after ππ* excitation: (a) trajectories that rapidly decay (within 20 fs) to the S_1 state; (b) trajectories that are still in the S_2 state after 20 fs.

the *trans* → *cis* isomerisation.[24,33] While there are not enough trajectories that follow this pathway to be able to extract reliable lifetimes, the general trend of these trajectories can be determined by examining times of hops between states. As stated previously the hops to S_3 occur within the first 20 fs, while the subsequent $S_3 \to S_2$ hops take place at an average time of 46 fs. After this, the pathway followed is essentially equivalent to the pathway followed by trajectories that remain in S_2 for at least 20 fs. We therefore conclude that the $S_2 \to S_3$ transfer has little direct effect on the overall photoisomerisation mechanism. However, the presence of this S_3 state in the simulation possibly reduces the number of trajectories which can follow the first electronic pathway (rapidly decaying from $S_2 \to S_1$), and so it is still important to include this pathway in simulations.

3.2 Structural dynamics

In order to better understand the isomerisation, let us discuss the dynamics in more detail, examining internal coordinates and geometries at which hops between electronic states occur. Fig. 3 shows the changes in the central C–N=N–C angle and in the central N=N bond length. From these it is clear that the mechanism of isomerisation is rotation-based, with the CNNC dihedral reaching −90° within 50 fs for almost all trajectories. This is in agreement with previous computational studies of the isomerisation mechanism.[18,20] There is a clear preference for direction of rotation due to steric hindrance of the phenyl rings, with rotation towards negative dihedral angles preferred. This is defined in previous works as the anticlockwise direction and shown visually in Fig. S2 in the ESI.†[37] The full inversion mechanism can be rejected, since the CNN angles do not typically exceed 160° and the average CNN angle barely changes (see Fig. S8 in the ESI†) – in the inversion isomerisation mechanism one (or both) of the CNN angles would pass through 180°.

From examination of some sample isomerising trajectories (of which some typical examples are given as movies in the ESI†), the mechanism can be more clearly understood. Excluding a handful (around 5%) of trajectories which rotate in the unfavourable clockwise direction, the first step that the trajectories

follow is a rapid change in the central C–N=N–C dihedral, rotating anticlockwise from the starting value of around −3.5° to *ca.* −90° within the first 50 fs (Fig. 3).

From this point, the ensemble splits into three main groups of trajectories; (i) some trajectories rotate back towards 0 within the next 100 fs and, as a result, reform the *cis* isomer – these are non-reactive trajectories; (ii) some trajectories continue to rotate past −90° immediately, reaching around −180° in around 150° additional fs to form the *trans* isomer; and (iii) a smaller number of trajectories oscillate around −90° for some time (>100 fs) after the initial fast rotation to −90°. These trajectories can form either the *cis* or *trans* isomer, although the *trans* isomer is preferentially formed.

While the initial rotation to −90° is the same for both excitations, the differences between the two ensembles of photochromes begin to appear after this point (*ca.* 50 fs), in the splitting of trajectories into these three categories. More specifically, the major difference is seen in the number of trajectories which pass through −90° and proceed immediately to the *trans* isomer, *versus* those which remain around −90° for a significant period of time (>100 fs) – this is visually clear in Fig. 3(a) and (b). The percentage of photochromes that follow each pathway when starting in the nπ* (S_1) and the ππ* (S_2) states respectively are given in Table 2. These values are obtained by counting the number of trajectories in each pathway (determined by central C–N=N–C dihedral) at time 170 fs.

The major difference seen between the dynamics initiated in the two different states is the number of trajectories that remain stuck around −90° instead of continuing rotation to −180° and consequently forming *trans*-AZB. More than twice as many trajectories are trapped around −90° when starting from the ππ* state, and they are also trapped around −90° for a longer period of time – on average ∼100 fs longer.

We can conclude that the major pathways followed after excitation are the same, with the differences between the two excitations mainly being in the splitting of trajectories, *i.e.*, the percentage of photochromes which follow each pathway. The plot starting in the to ππ* state is also more noisy than starting in the lower energy nπ* state, as expected due to the higher
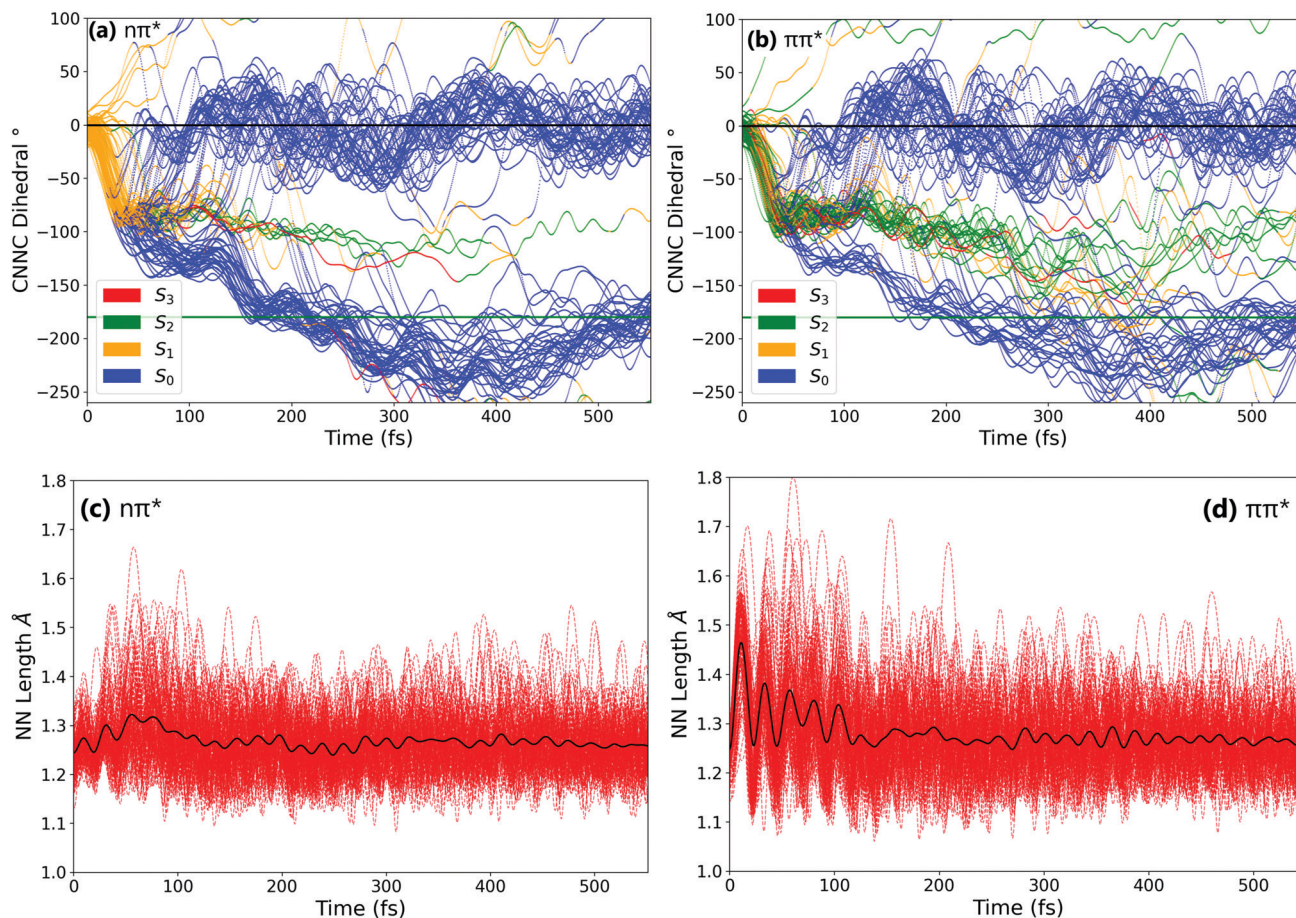
Fig. 3 Evolution of selected internal coordinates – (a) and (b) C–N=N–C dihedral and (c) and (d) N=N bond – throughout the simulations after (a) and (c) nπ* excitation, or (b) and (d) ππ* excitation. Colouring of (a) and (b) represents the active state of each trajectory at each timestep – active state colouring is excluded for visual clarity from figures (c) and (d). Horizontal lines in (a) and (b) indicate the *cis* (black) and *trans* (green) isomers. The solid black lines in (c) and (d) represent the average N=N bond length across all trajectories.

Table 2 Splitting of trajectories after the initial rapid rotation to C–N=N–C = −90° obtained at time 170 fs

	cis (%)	*trans* (%)	S_2 trapping (%)
$S_1(n\pi^*)$ excitation	42	37	14
$S_2(\pi\pi^*)$ excitation	43	19	31

energy of the system. Another major difference between nπ* and ππ* excitations is that the latter is accompanied by a significant activation of the N=N stretching mode, not seen in the former; see Fig. 3(c) and (d).

In order to characterise the dynamics relating to the trajectories that follow each of the pathways, the trajectories for the C–N=N–C dihedral plots in Fig. 3(a) and (b) are coloured to represent the state that each trajectory is in at each timestep. It can be seen that the trajectories that remain stuck around −90° are mostly in the S_2 state. In fact, after S_1 excitation, the trajectories 'trapped' around −90° for a significant time are those that have undergone a back-hop from $S_1 \rightarrow S_2$ and are in the S_2 state around −90°. This 'trapping' should therefore be related to the shape of the S_2 potential energy surface. By carrying out a fixed geometry scan (Fig. S3 and S4 in the ESI†) along the central

C–N=N–C coordinate, the shape of the potential energy surfaces in this rotational coordinate was characterised. The shape of these potential energy surfaces support this 'trapping', with a minimum in S_2 for a dihedral close to −90°, as well as a larger gap between the S_2 and S_1 surfaces compared to that between the S_1 and S_0. The molecules that remain around −90° in the S_2 state can be interpreted as becoming trapped in a potential well, oscillating around this point in other coordinates. This possibility of trapping after ππ* excitation in a S_2 rotational potential well was also reported by Zhu *et al.*[20]

On escaping this potential well, the $S_2 \rightarrow S_1$ hops occur at an average C–N=N–C dihedral angle of −93.1°, with a minimal spread around this average value – see the distribution of the dihedral of hops in Fig. S10 in the ESI.† The $S_2 \rightarrow S_1$ hops do not generally occur around the optimised S_2/S_1 conical intersection (CI, geometry given in ESI†) which has a central C–N=N–C value of −59.9°, nor around the other optimised S_2/S_1 CI found by Zhu *et al.*[20] at −132°.

Based on the optimised CIs and on transient absorption data, some others have previously proposed that isomerisation can occur *via* S_2/S_1 conical intersections, with the final *trans* isomer being formed in the S_1 state.[16,20] We do indeed find this
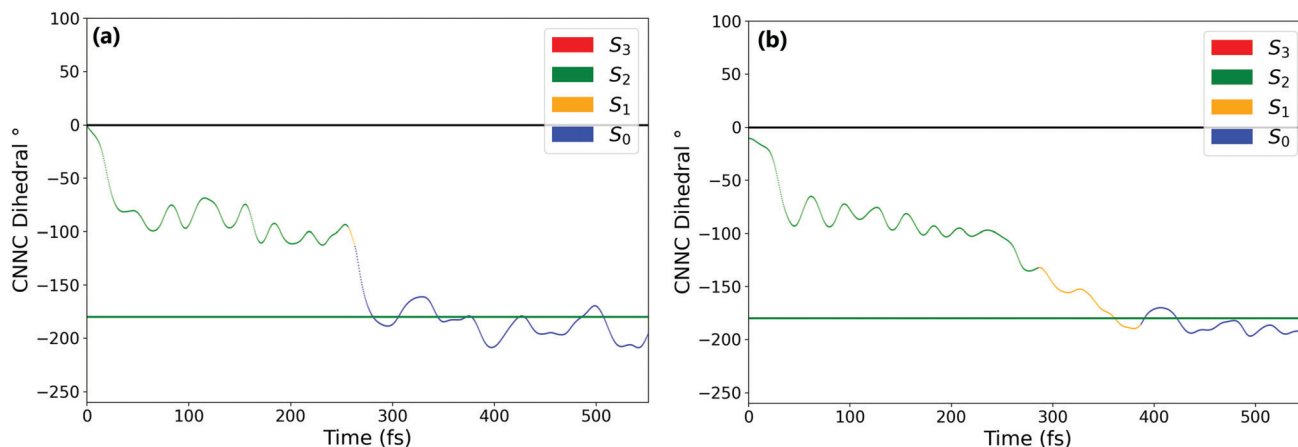
19160 | *Phys. Chem. Chem. Phys.*, 2021, **23**, 19155–19165

This journal is © the Owner Societies 2021

Fig. 4 Example of the two types of trajectory that leave the S_2 well after $\pi\pi^\star$ excitation. (a) Leaves the S_2 well *via* rapid consecutive $S_2 \rightarrow S_1 \rightarrow S_0$ intersections, all located around $-90°$, (b) leaves the S_2 well *via* $S_2 \rightarrow S_1$ intersection around $-90°$ but isomerises to *trans*-AZB before $S_1 \rightarrow S_0$ decay. Horizontal lines indicate the *cis* (black) and *trans* (green) isomers.

in our simulations, however only for a fraction (8%) of overall photochromes excited to S_2. The isomer formed for the trajectories that remain trapped on the S_2 surface is mostly determined by the rotational path taken after the ensuing $S_1 \rightarrow S_0$ hop: for 73% of photochromes trapped on S_2 (21% of all $\pi\pi^\star$ trajectories), $S_1 \rightarrow S_0$ hopping occurs almost immediately after $S_2 \rightarrow S_1$. This $S_1 \rightarrow S_0$ hopping also occurs around the same dihedral value, with an average of $-93.3°$. However, for the remaining 27% of photochromes trapped in S_2 (8% of all $\pi\pi^\star$ trajectories), the $S_1 \rightarrow S_0$ hop does not occur until later in the simulation, when the central C–N=N–C dihedral has reached around $180°$. The difference between these two cases is illustrated in Fig. 4. In the first case Fig. 4(a), the trajectory spends only 6 fs in the S_1 state after $S_2 \rightarrow S_1$ hopping, $S_1 \rightarrow S_0$ hopping occurs almost immediately. However, in the second case Fig. 4(b), the isomerisation has indeed taken place *via* the S_2/S_1 conical intersection (which is typically at angles rotated past $-90°$) and the *trans* isomer is present in its S_1 state. This is consistent with the presence of excited state absorption (ESA) bands attributed to *trans*-AZB in the study of Quick *et al.*[16] Since for these 8% of overall photochromes the *trans* isomer formed by photoisomerisation is formed in the $n\pi^\star$ S_1 excited state, ESA bands of the *trans*-AZB would be expected to appear after around 250 fs based on our simulations. This is again closely in line with these experimentally measured ESA bands, which in fact begin to appear at times >200 fs.[16]

A summary of the important pathways followed by *cis*-AZB after $n\pi^\star$ and $\pi\pi^\star$ excitation that have been described in this section is given in Fig. 5, along with the fraction of photochromes which follow each pathway.

3.3 Quantum yields

3.3.1 Comparison to recent experimental values. In order to calculate quantum yields, one needs a method for assigning trajectories as either reactive or non-reactive – that is, forming *trans*-AZB or *cis*-AZB respectively. We determine this by whether the central C–N=N–C angle passes $180°$. There are some

trajectories that pass through $180°$ and continue to rotate back to $360°$, but in a more realistic simulation energy loss to the solvent/bath would mostly prevent this from happening. We therefore assume that if a value of CNNC = $180°$ is reached the trajectory can be treated as reactive, forming *trans*-AZB. This also assigns the few trajectories still trapped in the S_2 well at the end of the simulation as *cis*-AZB – from examination of the evolution of these trajectories, this can be justified as the dihedral angle in all remaining trajectories of this type are in the process of rotating back to *cis*-AZB. A more detailed validation of the method used to assign reactive *versus* non-reactive trajectories can be found in the ESI† (Fig. S9).

The calculated quantum yields $\phi_{c \rightarrow t}$ we therefore obtain from these simulations are 0.57 for the $n\pi^\star$ (S_1) excitation, and 0.47 for the $\pi\pi^\star$ (S_2) excitation. These quantum yields are in line with those obtained in the previous computational study of Persico *et al.*,[18] with both quantum yields higher than typically obtained in experiment (see Table 1). The higher quantum yield after $n\pi^\star$ excitation compared to $\pi\pi^\star$ excitation is successfully reproduced by our simulations. The difference between our two calculated quantum yields is 0.10 only – exciting to the $\pi\pi^\star$ state only results in a slight reduction in quantum yield. This is in line with the most recent measurements of Ladányi *et al.*, who measured a difference in QYs of 0.11. Our theoretical results therefore support these more recent measurements, rather than the previously accepted quantum yields which showed the quantum yield decreasing by up to a factor of two on exciting to $\pi\pi^\star$.

It is noted that the solvent used in experiments is expected to influence the yield of the photoisomerization reaction (see Table 1). While our simulations reproduce quantitatively the difference in QYs between the two excitations, it fails at reproducing the absolute individual QYs of the two excitations. A source of error might be the omission of the solvent in the simulation, but including explicit solvent molecules is beyond the scope of the present study.

3.3.2 Testing the prior mechanistic assumption. Having tackled the first aim of this study, with the difference in QY fitting best with the most recent measurements, we move on to
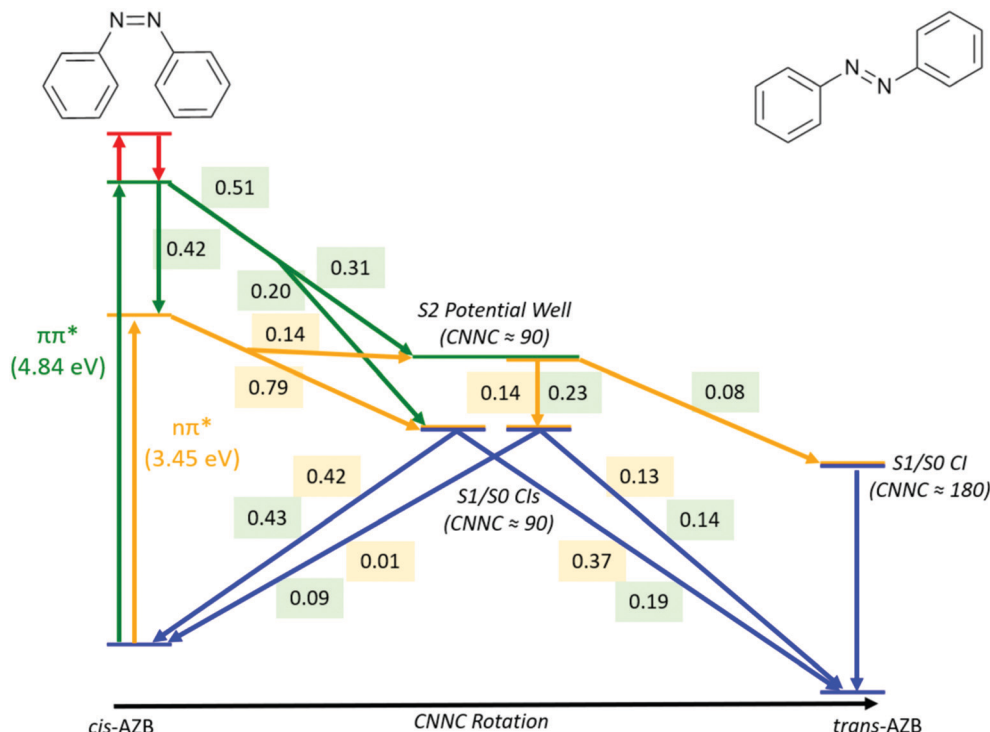
This journal is © the Owner Societies 2021

Phys. Chem. Chem. Phys., 2021, **23**, 19155–19165 | **19161**

Fig. 5 Summary of major pathways, and the fraction of trajectories which follow each pathway, accessible to *cis*-AZB upon excitation to the nπ* (numbers in yellow) and ππ* (numbers in green) states.

our next aim. This was to test the assumption that the same mechanism explains the reduction in quantum yield when exciting to the ππ* state for *cis* → *trans* isomerisation as for *trans* → *cis*.

The commonly accepted *trans* → *cis* mechanism for the reduction of quantum yield is as follows:[18,29,30] on exciting to the ππ* (S_2) state of *trans*-AZB, additional vibrational energy is given to the C–N═N bending modes. This additional energy allows for $S_1 \to S_0$ decay through a higher energy section of the S_1/S_0 intersection seam, located earlier along the central CNNC torsional coordinate. To test if this holds for *cis* → *trans* isomerisation, let us look at the geometries at which $S_1 \to S_0$ hopping occurs according to the surface hop algorithm used – these geometries can be interpreted as the points on the intersection seam at which decay takes place.

Fig. 6 compares the C–N═N–C dihedral angle and potential energy of the $S_1 \to S_0$ hops for both initial excitations. From this figure, it is clear that the $S_1 \to S_0$ hops are mostly located around −85° after both S_1 and S_2 excitations, and while the hops after S_2 excitation are spread over a larger range of angles, they do not on average occur earlier along the central C–N═N–C torsion coordinate.

The average dihedral values for the $S_1 \to S_0$ hops could be obtained by integrating along the dihedral coordinate and fitting to a logistic function, and are listed in Table 3. They are almost perfectly equivalent for both excitations, although the S_1/S_0 hops do clearly occur at higher potential energies after S_2 excitation than after S_1. Besides this, the most significant differences are seen in the length of bonds, with bond lengths in general being slightly longer for the ππ* case.

Unlike for the *trans* → *cis* isomerisation, in which the rotation around the central CNNC occurs slowly after excitation, the *cis* isomer rotation occurs much faster. The previous study by Persico *et al.* found that after S_1 and S_2 excitation of *trans*-AZB, the −90° point was reached after around 400 and 900 fs respectively.[18] In comparison, in the same study the −90° point was reached after only 75 and 100 fs for the *cis*-AZB S_1 and S_2 excitations respectively.

From scans along the CNNC torsional coordinate (keeping all other coordinates fixed), starting from either the *cis* or the *trans* isomer (Fig. S4 in ESI†), the reason for this is clear. The gradient of the slope of the S_1 surface along the torsional coordinate is greater for *cis*-AZB than *trans*-AZB, and the S_2 surface is also sloped towards −90° for *cis*-AZB, while the S_2 state appears at a minimum along the torsional coordinate for *trans*-AZB. The rotation is therefore significantly faster after S_1 excitation for *cis versus trans* – it takes around 50 fs for *cis* to rotate to −90° in our simulations. Exciting to S_2 also immediately drives the favourable rotation for *cis*-AZB, while for *trans*-AZB the rotation is not activated by S_2 excitation.

So, instead of bending modes allowing access to higher energy sections of the S_1/S_0 CI seam while the molecule slowly rotates about the CNNC coordinate, the rotation brings the molecule towards −84° (the average hopping angle) too fast for bending modes to allow access to earlier sections of the CI seam when starting from *cis*-AZB. As a result the hopping occurs almost exclusively close to the fully twisted geometry (CNNC of *ca.* −90°) after both nπ* or ππ* excitation.

3.3.3 Insights into the quantum yield wavelength-dependency. Since the reduction in quantum yield on exciting with shorter

19162 | *Phys. Chem. Chem. Phys.*, 2021, **23**, 19155–19165

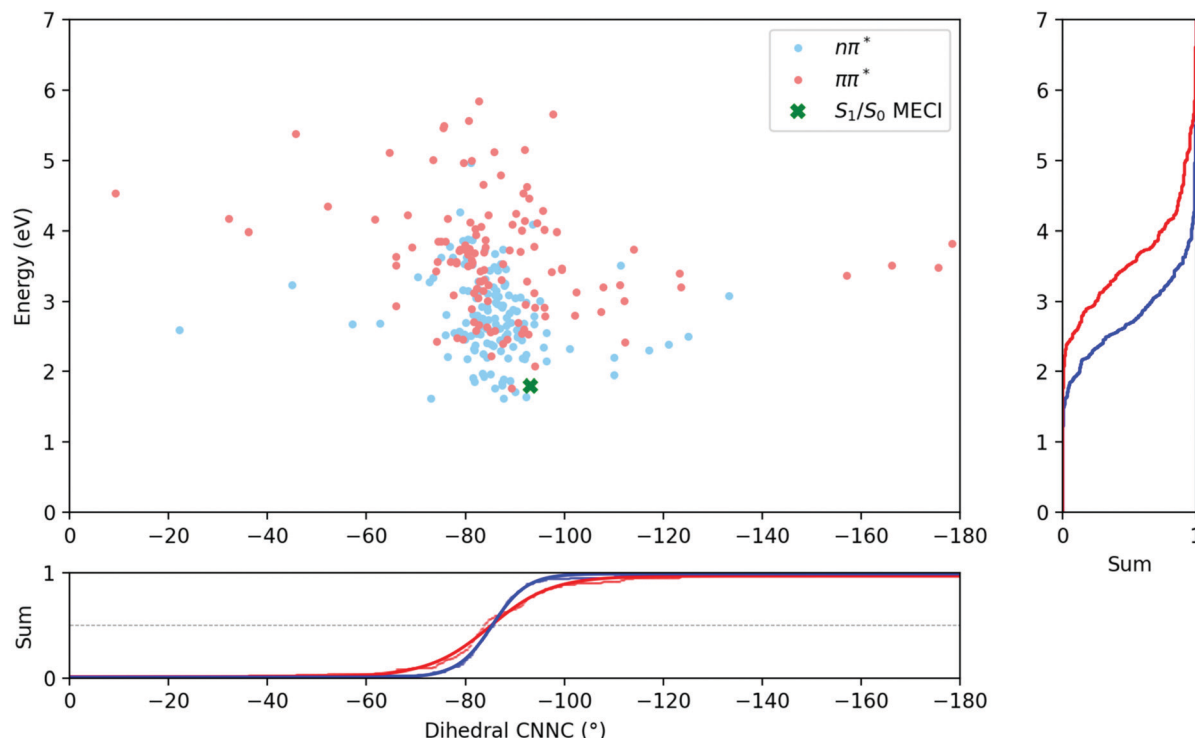This journal is © the Owner Societies 2021

Fig. 6 Energies and dihedral angles of the $S_1 \rightarrow S_0$ hopping geometries after excitation to the $n\pi^*$ (S_1) (in blue) and $\pi\pi^*$ (S_2) (in red) states. The position of the S_1/S_0 minimum energy conical intersection is indicated by a green cross.

Table 3 Comparison of average values of selected properties of the $S_1 \rightarrow S_0$ hopping geometries after excitation to the $n\pi^*$ and $\pi\pi^*$ states

Property	$S_1(n\pi^*)$ excitation	$S_2(\pi\pi^*)$ excitation
Energy (eV)	2.76	3.59
CNNC dihedral (°)	−85.4	−85.2
Average CNN angle (°)	123.4	124.5
CNN asymmetry (°)	19.9	19.6
NN length (Å)	1.25	1.26
Average CN length (Å)	1.41	1.43
CN difference (Å)	0.07	0.09

wavelengths to the higher energy state can not be attributed to $S_1 \rightarrow S_0$ hopping at lower central C–N=N–C angles, another mechanism must explain the reduction in yield. As we have been able to reproduce the experimentally measured[17] reduction in quantum yield, our simulations should offer physical insight into the mechanism behind this reduction in QY.

As previously described, the main difference between exciting to the $n\pi^*$ and the $\pi\pi^*$ states is the splitting of trajectories after the initial rotation to −90°. In particular, as given in Table 2 the number of trajectories that either remain around −90° for a significant period of time or pass straight through −90° towards the *trans* isomer is markedly different. The number of trajectories that rotate back to *cis*-AZB or rotate clockwise is almost identical in both excitation cases.

From Table 2, we can establish that the difference upon exciting to the $\pi\pi^*$ state is that there are 16–17% of trajectories, which under $n\pi^*$ excitation would have immediately formed *trans*-AZB, that are instead trapped in the S_2 well. These trajectories can

proceed to either *cis*-AZB or *trans*-AZB therefore lowering the quantum yield. However, only 35% of the $\pi\pi^*$ trajectories trapped in the well in fact reform *cis*-AZB, so we would only expect a reduction in QY on $\pi\pi^*$ excitation of around 0.05 from this, instead of the calculated reduction of 0.10. There is therefore a second factor which contributes to the QY reduction.

Upon further examination of the trajectories trapped in the S_2 well, the 12% that are trapped after $n\pi^*$ excitation are in fact still associated with the S_2 state, and result from back-hops from S_1 to S_2 around −90°. However, these trajectories leave the S_2 well earlier in time than those trapped after $\pi\pi^*$ excitation. These trajectories overwhelmingly result in *trans*-AZB – only 9% of trapped $n\pi^*$ trajectories form *cis*-AZB.

So the reduction in QY can be attributed to two factors related to the trapping on the S_2 state around −90°: (i) more photochromes are trapped around −90° after $\pi\pi^*$ excitation, and (ii) photochromes trapped around −90° after $\pi\pi^*$ excitation are roughly 4 times more likely to form *cis*-AZB than those trapped after $n\pi^*$ excitation. Since the splitting from the trapping well is different after both excitations, we expect there to be some differences between the two excitation cases in the geometries explored during this pathway. Unfortunately, we do not have enough trajectories that follow this pathway (in particular after $n\pi^*$ excitation) to be able to carry out a reasonable statistical analysis.

4 Conclusions

We have studied the *cis* → *trans* isomerisation mechanism of azobenzene after $n\pi^*$ and $\pi\pi^*$ excitations, using high-level *ab*

initio mixed quantum-classical dynamics, and have demonstrated that our simulations are able to reproduce the trend in quantum yields obtained in the most recent experiments. More specifically, we have determined a decrease in quantum yield of 0.10, from $\phi_{c \to t} = 0.57$ after $n\pi^*$ excitation to $\phi_{c \to t} = 0.47$ after $\pi\pi^*$ excitation. While this is different from previously accepted literature values (as given in Table 1) with measured decreases in quantum yield of up to 0.32,[14] it is consistent with the recently measured drop of 0.11.[17] Our simulations therefore support these most recent measurements of the quantum yields of azobenzene *cis* → *trans* photoisomerisation.

We have tested the mechanism for the reduction in quantum yield, as previous studies have typically assumed the reasoning behind lower quantum yields measured at shorter wavelength is the same for both photoisomerisation directions – in other words, it was assumed that the mechanism determined for *trans* → *cis* photoisomerisation of AZB also applies to the *cis* → *trans* direction.[18,24,35] Instead we have found that, unlike for *trans* → *cis* photoisomerisation, in the *cis* → *trans* case there is no distinct difference between the central C–N=N–C angle of the geometries at which $S_1 \to S_0$ decay occurs when exciting to both $n\pi^*$ and $\pi\pi^*$ states. As a result our calculations do not support the *trans* → *cis* mechanism of $S_1 \to S_0$ decay occurring at higher energy areas of the conical intersection seam, located earlier along the coordinate of rotation about the central C–N=N–C dihedral angle. We have explained the absence of this mechanism in *cis* → *trans* isomerisation by the immediate activation of the rapid central rotational coordinate for both excitations, reaching *ca.* $-90°$ too fast to allow for exploration of the $S_1 \to S_0$ seam along the rotation.

In fact, the rotation occurs on such a timescale that for 51% of photochromes excited to the $\pi\pi^*$ state the rotation in fact occurs before $S_2 \to S_1$ decay, which occurs close to $-90°$. For the majority of these photochromes the photoreaction product is still determined by the path taken through a subsequent $S_1 \to S_0$ intersection around $-90°$, but for 8% of all photochromes excited to $\pi\pi^*$ the isomerisation pathway followed involves $S_1 \to S_0$ decay around $180°$, *i.e.*, after isomerisation to *trans*-AZB. For these 8% of photochromes, the photoisomerisation can conclusively be said to have occurred *via* the $S_2 \to S_1$ intersection around $-90°$ as predicted by Quick *et al.*[16]

After rejecting the equivalent QY reduction mechanism acting in *trans* → *cis* isomerisation, we have instead attributed the reduction of the QY on exciting to the $\pi\pi^*$ state compared to $n\pi^*$ to a potential well on the S_2 surface, located around C–N=N–C = $-90°$ and accessible after both $n\pi^*$ and $\pi\pi^*$ excitation. Upon leaving this well either *cis* or *trans*-AZB may be formed. Two factors relating to this potential well have been found to contribute to the QY reduction: (i) a fraction of photochromes which under $n\pi^*$ excitation would have exclusively formed *trans*-AZB were instead trapped in this well after $\pi\pi^*$ excitation, and (ii) photochromes in this well had been excited to the $\pi\pi^*$ state were also found to be more likely than those excited to the $n\pi^*$ state to reform *cis*-AZB upon leaving the well. Our measured reduction in QY of 0.10 thus emerges from the combination of these two factors.

Conflicts of interest

There are no conflicts to declare.

Acknowledgements

References

1 A. A. Beharry and G. A. Woolley, *Chem. Soc. Rev.*, 2011, **40**, 4422–4437.
2 J. Kumar, L. Li, X. L. Jiang, D.-Y. Kim, T. S. Lee and S. Tripathy, *Appl. Phys. Lett.*, 1998, **72**, 2096–2098.
3 S. Crespi, N. A. Simeth and B. König, *Nat. Rev. Chem.*, 2019, **3**, 133–146.
4 M. Zhu and H. Zhou, *Org. Biomol. Chem.*, 2018, **16**, 8434–8445.
5 M. Böckmann, N. L. Doltsinis and D. Marx, *J. Phys. Chem. A*, 2010, **114**, 745–754.
6 H. Rau and E. Lueddecke, *J. Am. Chem. Soc.*, 1982, **104**, 1616–1620.
7 I. K. Lednev, T. Q. Ye, L. C. Abbott, R. E. Hester and J. N. Moore, *J. Phys. Chem. A*, 1998, **102**, 9161–9166.
8 C. Nonnenberg, H. Gaub and I. Frank, *ChemPhysChem*, 2006, **7**, 1455–1461.
9 H. M. Bandara and S. C. Burdette, *Chem. Soc. Rev.*, 2012, **41**, 1809–1825.
10 J. Calbo, C. E. Weston, A. J. White, H. S. Rzepa, J. Contreras-Garca and M. J. Fuchter, *J. Am. Chem. Soc.*, 2017, **139**, 1261–1274.
11 G. Zimmerman, L.-Y. Chow and U.-J. Paik, *J. Am. Chem. Soc.*, 1958, **80**, 3528–3531.
12 S. Malkin and E. Fischer, *J. Phys. Chem.*, 1962, **66**, 2482–2486.
13 J. Ronayette, R. Arnaud, P. Lebourgeois and J. Lemaire, *Can. J. Chem.*, 1974, **52**, 1848–1857.
14 P. Bortolus and S. Monti, *J. Phys. Chem.*, 1987, **91**, 5046–5050.
15 G. Gauglitz and S. Hubig, *J. Photochem.*, 1985, **30**, 121–125.
16 M. Quick, A. L. Dobryakov, M. Gerecke, C. Richter, F. Berndt, I. N. Ioffe, A. A. Granovsky, R. Mahrwald, N. P. Ernsting and S. A. Kovalenko, *J. Phys. Chem. B*, 2014, **118**, 8756–8771.
17 V. Ladányi, P. Dvořák, J. A. Anshori, Ĺ. Vetráková, J. Wirz and D. Heger, *Photochem. Photobiol. Sci.*, 2017, **16**, 1757–1761.
18 C. Ciminelli, G. Granucci and M. Persico, *Chem. – Eur. J.*, 2004, **10**, 2327–2341.
19 L. Yu, C. Xu, Y. Lei, C. Zhu and Z. Wen, *Phys. Chem. Chem. Phys.*, 2014, **16**, 25883–25895.
20 L. Yu, C. Xu and C. Zhu, *Phys. Chem. Chem. Phys.*, 2015, **17**, 17646–17660.
21 C. E. Weston, R. D. Richardson, P. R. Haycock, A. J. White and M. J. Fuchter, *J. Am. Chem. Soc.*, 2014, **136**, 11878–11881.
22 D. Bléger, J. Schwarz, A. M. Brouwer and S. Hecht, *J. Am. Chem. Soc.*, 2012, **134**, 20597–20600.

19164 | *Phys. Chem. Chem. Phys.*, 2021, **23**, 19155–19165

This journal is © the Owner Societies 2021

23 L. N. Lameijer, S. Budzak, N. A. Simeth, M. J. Hansen, B. L. Feringa, D. Jacquemin and W. Szymanski, *Angew. Chem., Int. Ed.*, 2020, **59**, 21663–21670.

24 I. Conti, M. Garavelli and G. Orlandi, *J. Am. Chem. Soc.*, 2008, **130**, 5216–5230.

25 Y. Ootani, K. Satoh, A. Nakayama, T. Noro and T. Taketsugu, *J. Chem. Phys.*, 2009, **131**, 194306.

26 A. Warshel, *Nature*, 1976, **260**, 679–683.

27 R. S. Liu and A. E. Asato, *Proc. Natl. Acad. Sci. U. S. A.*, 1985, **82**, 259–263.

28 H. Rau, in *Photochromism*, ed. H. Dürr and H. Bouas-Laurent, Elsevier Science, Amsterdam, 2003, pp. 165–192.

29 A. Nenov, R. Borrego-Varillas, A. Oriana, L. Ganzer, F. Segatta, I. Conti, J. Segarra-Marti, J. Omachi, M. Dapor, S. Taioli, C. Manzoni, S. Mukamel, G. Cerullo and M. Garavelli, *J. Phys. Chem. Lett.*, 2018, **9**, 1534–1541.

30 F. Aleotti, L. Soprani, A. Nenov, R. Berardi, A. Arcioni, C. Zannoni and M. Garavelli, *J. Chem. Theory Comput.*, 2019, **15**, 6813–6823.

31 T. Ishikawa, T. Noro and T. Shoda, *J. Chem. Phys.*, 2001, **115**, 7503–7512.

32 S. Yuan, Y. Dou, W. Wu, Y. Hu and J. Zhao, *J. Phys. Chem. A*, 2008, **112**, 13326–13334.

33 J. Casellas, M. J. Bearpark and M. Reguero, *ChemPhysChem*, 2016, **17**, 3068–3079.

34 C. Xu, L. Yu, F. L. Gu and C. Zhu, *Phys. Chem. Chem. Phys.*, 2018, **20**, 23885–23897.

35 A. Cembran, F. Bernardi, M. Garavelli, L. Gagliardi and G. Orlandi, *J. Am. Chem. Soc.*, 2004, **126**, 3234–3243.

36 L. Gagliardi, G. Orlandi, F. Bernardi, A. Cembran and M. Garavelli, *Theor. Chem. Acc.*, 2004, **111**, 363–372.

37 M. Pederzoli, J. Pittner, M. Barbatti and H. Lischka, *J. Phys. Chem. A*, 2011, **115**, 11136–11143.

38 L. Ye, C. Xu, F. L. Gu and C. Zhu, *J. Comput. Chem.*, 2020, **41**, 635–645.

39 S. Monti, G. Orlandi and P. Palmieri, *Chem. Phys.*, 1982, **71**, 87–99.

40 Ĺ. Vetráková, V. Ladányi, J. Al Anshori, P. Dvořák, J. Wirz and D. Heger, *Photochem. Photobiol. Sci.*, 2017, **16**, 1749–1756.

41 B. O. Roos, P. R. Taylor and P. E. Sigbahn, *Chem. Phys.*, 1980, **48**, 157–173.

42 B. O. Roos, R. Lindh, P.-Å. Malmqvist, V. Veryazov and P.-O. Widmark, *J. Phys. Chem. A*, 2004, **108**, 2851–2858.

43 F. Aquilante, R. Lindh and T. Bondo Pedersen, *J. Chem. Phys.*, 2007, **127**, 114107.

44 Y. Harabuchi, M. Ishii, A. Nakayama, T. Noro and T. Taketsugu, *J. Chem. Phys.*, 2013, **138**, 064305.

45 K. Andersson, P. A. Malmqvist, B. O. Roos, A. J. Sadlej and K. Wolinski, *J. Phys. Chem.*, 1990, **94**, 5483–5488.

46 M. Barbatti, M. Ruckenbauer, F. Plasser, J. Pittner, G. Granucci, M. Persico and H. Lischka, *Wiley Interdiscip. Rev.: Comput. Mol. Sci.*, 2014, **4**, 26–33.

47 I. F. Galván, M. Vacher, A. Alavi, C. Angeli, F. Aquilante, J. Autschbach, J. J. Bao, S. I. Bokarev, N. A. Bogdanov, R. K. Carlson, L. F. Chibotaru, J. Creutzberg, N. Dattani, M. G. Delcey, S. S. Dong, A. Dreuw, L. Freitag, L. M. Frutos, L. Gagliardi, F. Gendron, A. Giussani, L. González, G. Grell, M. Guo, C. E. Hoyer, M. Johansson, S. Keller, S. Knecht, G. Kovačević, E. Källman, G. Li Manni, M. Lundberg, Y. Ma, S. Mai, J. P. Malhado, P. Å. Malmqvist, P. Marquetand, S. A. Mewes, J. Norell, M. Olivucci, M. Oppel, Q. M. Phung, K. Pierloot, F. Plasser, M. Reiher, A. M. Sand, I. Schapiro, P. Sharma, C. J. Stein, L. K. Sørensen, D. G. Truhlar, M. Ugandi, L. Ungur, A. Valentini, S. Vancoillie, V. Veryazov, O. Weser, T. A. Wesołowski, P.-O. Widmark, S. Wouters, A. Zech, J. P. Zobel and R. Lindh, *J. Chem. Theory Comput.*, 2019, **15**, 5925–5964.

48 J. C. Tully, *J. Chem. Phys.*, 1990, **93**, 1061–1071.

49 S. Hammes-Schiffer and J. C. Tully, *J. Chem. Phys.*, 1994, **101**, 4657–4667.

50 G. Granucci and M. Persico, *J. Chem. Phys.*, 2007, **126**, 134114.

51 The number of trajectories in the S_3 state at this time is too low to obtain resolved electronic state populations.

This journal is © the Owner Societies 2021

Phys. Chem. Chem. Phys., 2021, **23**, 19155–19165 | **19165**